Splitting of microcavity degenerate modes in rotating photonic crystals—the miniature optical gyroscopes

Ben Z. Steinberg and Amir Boag

School of Electrical Engineering, Tel Aviv University, Ramat-Aviv, Tel Aviv 69978, Israel

A manifestation of the Sagnac effect in a rotating photonic crystal that contains a microcavity with degenerate modes is explored. It is shown that generally rotation can cause the resonance frequency to split into M different frequencies, where M is the order of the stationary-system mode degeneracy. The results are derived using a new rotation-induced eigenvalue theory that holds for any two-dimensional or three-dimensional rotating microcavity with mode degeneracy. Comparison with exact numerical simulations of the rotating system is provided. Miniature optical gyroscopes are discussed. © 2006 Optical Society of America

OCIS codes: 120.5790, 230.5750.

1. INTRODUCTION

In a recent publication[1] the effect of rotation on a photonic crystal (PhC) containing a set of microcavities has been studied analytically. The configuration consisted of a coupled-cavity waveguide (CCW), known also as a coupled-resonator optical waveguide (CROW), situated along a circular path within an otherwise perfect crystal. To our knowledge, novel manifestation of the Sagnac effect, expressed via a rotation-dependent dispersion equation, has been reported. This effect is shown to depend on new sets of parameters not previously reported or studied as far as we know and is intimately related to the intricate scattering–propagation phenomena associated with propagation in crystals and microcavities. Although the specific examples have been presented for PhC structures, the general analysis, as well as the resulting dispersion relation, holds for a general CCW structure.

From a somewhat broader point of view, the previously reported results[1] indicate that the added flexibility and ability of PhCs to manipulate light may offer new insights into the basic understanding of the Sagnac effect and reveal new phenomena. From the practical point of view, this can potentially lead to novel designs and to a new generation of optical gyroscopes.

To that end, the general purpose of the present work is twofold. Our first goal is to further explore the effect of rotation in PhC microcavities; we study cavities with mode degeneracy and point out their potential for optical gyroscopes. To the best of the authors' knowledge, these miniature structures constitute the smallest optical gyroscopes known so far. This study is based on extending the cavity perturbation theory of degenerate modes[2] to rotating PhCs. The second goal is to use the Green's function theory for a rotating medium[3] in order to validate numerically our theoretical results.

We feel, however, that before turning to the theoretical study, a brief description of the differences between our work and the classical analysis of the Sagnac effect is in order. The simplest and most familiar example of an optical resonator with degenerate modes is the closed loop or ring structure made out of a conventional (reciprocal) material. Here, mode degeneracy is manifested by the fact that, for any of its resonant frequencies, the ring supports two modes propagating in opposite directions. If a ring of radius R rotates at an angular velocity Ω around an arbitrary axis normal to the ring plane, reciprocity along the propagation path is lost; the degenerate resonant frequency splits into two distinct frequencies $\omega^{(1,2)} = \omega_0 \pm \Omega \omega_0 R/nc$ corresponding to propagation in counter-rotation or corotation directions. This is nothing but the classical Sagnac effect.[4] However, there are many cases of mode degeneracy associated with microcavities in PhCs, for which the manifestation of the Sagnac effect is somewhat less obvious. An example is shown in Fig. 1. Consider a two-dimensional PhC that consists of dielectric cylinders of radius 0.6 μm and $\epsilon_r = 8.41$, situated on a hexagonal lattice with a lattice constant of $a = 4$ μm. For TM polarization, a microcavity with two degenerate modes at a resonant wavelength of $\lambda_0 = 2\pi c/\omega_0 = 8.79941$ μm is created by increasing the radius of a cylinder to 1.1 μm. The degenerate modes' electric field magnitude is shown in a logarithmic scale. Similar examples, but in TE polarization and slab geometry, are provided in the literature.[5,6] These modal fields cannot, in principle, be *a priori* presented as local plane waves or geometrical rays that propagate (and accumulate phase) along a well-defined path. Furthermore, in the general case the mode degeneracy rank M can be larger than 2 (i.e., in the general case the structure supports $M \geq 2$ distinct modal fields at its resonant frequency ω_0). Thus the classical formulation of the Sagnac effect, which holds for only two distinct modes and requires a precise definition of the propagation path, cannot be directly applied.

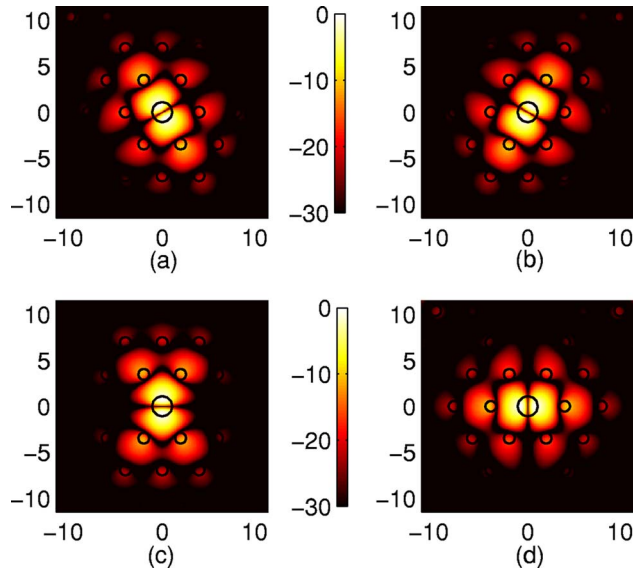As pointed out above, the first purpose of the present

Fig. 1. (Color online) Electric field magnitudes on a decibel scale of a doubly degenerate TM microcavity ($M=2$), in a two-dimensional hexagonal photonic crystal (PhC). The crystal is made of dielectric cylinders, outlined by black circles. (a) $\boldsymbol{E}_0^{(1)}$. (b) $\boldsymbol{E}_0^{(2)}$. These modes are nonorthogonal, and $\boldsymbol{E}_0^{(2)}$ is a $\pi/3$-rotated replica of $\boldsymbol{E}_0^{(1)}$. (c) The linear combination $\boldsymbol{E}_0^{(1)} \mapsto \boldsymbol{E}_0^{(1)} + \boldsymbol{E}_0^{(2)}$. (d) The linear combination $\boldsymbol{E}_0^{(2)} \mapsto \boldsymbol{E}_0^{(1)} - \boldsymbol{E}_0^{(2)}$. These modes are orthogonal.

work is to develop a general theory for the analysis of microcavities with mode degeneracy, under slow rotation conditions. The basic methodology is to extend the cavity perturbation theory of degenerate modes[2] to rotating PhCs, in their rest (noninertial) frame. The result is a formulation similar in structure to the classical cavity perturbation theory, in which the effect of rotation appears as a new perturbation operator. We solve our proposed equation and get closed-form expressions for the effect of rotation on the degenerate resonances. The formulation holds for a general cavity in a two- or three-dimensional configuration, and we show that in the specific case of a simple closed loop it precisely predicts the classical Sagnac effect.[4] In the more general case, we show that, under rotation, a resonance frequency ω_0 with mode degeneracy of rank $M \geq 2$ splits into M different resonances $\omega_\Omega^{(m)}(\Omega)$, $m=1 \ldots M$; the distance of each from ω_0 is proportional to the rotation rate Ω. We explore the general properties of these resonances (e.g., symmetries and central location) and provide explicit expressions for the splitting magnitude. Thus, in the specific case illustrated by Fig. 1, our general theory predicts a symmetrical splitting of the degenerate resonance into two distinct resonances $\omega_0 \pm \delta\omega(\Omega)$, where the splitting magnitude $\delta\omega(\Omega)$ is proportional to the system rotation rate Ω.

The structure of the paper is as follows. In Section 2, we develop the general theory and explore the symmetry properties of the splitting effect. In Section 3, we show that for the case of a simple ring structure our general theory reconstructs the classical Sagnac effect, and we suggest the concept of an effective rotation radius for the more general cavity. In Sections 4 and 5, we provide specific examples of splitting of degenerate modes in rotating PhC microcavities for a two-dimensional TM case and for

a TE slab model and compare our theoretical predictions with exact numerical computations. In Section 6, we present some observations pertaining to the implementation of rotating crystals and microcavities as optical gyroscopes. Concluding remarks are provided in Section 7.

2. THEORY

Let $\epsilon_r(\boldsymbol{r})$ be the (time-invariant) relative dielectric property of a stationary medium, as measured in its (inertial) rest frame. We assume now that the medium rotates slowly around the z axis at an angular radian velocity Ω:

$$\boldsymbol{\Omega} = \hat{z}\Omega. \tag{2.1}$$

The assumption of slow rotation implies that

(i) The angular velocity Ω and the PhC maximal dimension L satisfy $|\Omega L| \ll c$. Therefore no relativistic effects take place.
(ii) Consistent with the slow velocity assumption, no geometrical transformations or deformations take place. Thus, for example, the $\boldsymbol{\nabla}$ operator is conserved: $\boldsymbol{\nabla} = \boldsymbol{\nabla}'$. For the very same reason, time is invariant in both systems: $t = t'$.

As stated before, in this work we would like to solve the propagation of optical signal in the rotating-medium rest frame. According to a formal structure of electrodynamics, postulated in basic works[7,8] that served as the starting point to classical studies of the Sagnac effect,[9] the basic physical laws governing the electromagnetic fields are invariant under any coordinate transformation, including a noninertial one. The transformation to a rotating system is manifested only by an appropriate change of the constitutive relations. Therefore, under the slow rotation assumption discussed above, the source-free Maxwell's equations in the rotating frame are given by[7,8]

$$\boldsymbol{\nabla} \times \boldsymbol{E} = i\omega \boldsymbol{B}, \quad \boldsymbol{\nabla} \cdot \boldsymbol{B} = 0, \tag{2.2a}$$

$$\boldsymbol{\nabla} \times \boldsymbol{H} = -i\omega \boldsymbol{D}, \quad \boldsymbol{\nabla} \cdot \boldsymbol{D} = 0. \tag{2.2b}$$

Let the material properties at rest be given by ϵ, μ. Then up to the first order in velocity the constitutive relations in $\mathcal{R}$ take on the form[7]

$$\boldsymbol{D} = \epsilon \boldsymbol{E} - c^{-2}\boldsymbol{\Omega} \times \boldsymbol{r} \times \boldsymbol{H}, \tag{2.3a}$$

$$\boldsymbol{B} = \mu \boldsymbol{H} + c^{-2}\boldsymbol{\Omega} \times \boldsymbol{r} \times \boldsymbol{E}. \tag{2.3b}$$

In the above, c is the speed of light in vacuum, ω is the frequency, and a time dependence $\exp(-i\omega t)$ is assumed and suppressed. This set of Maxwell's equations has been used in the past as the starting point for studies of the Sagnac effect in classic works on optical gyroscopes.[9] We follow now the procedure outlined previously[1] to derive a wave equation governing the magnetic field. Substitute the above constitutive relations into Maxwell's equations (2.2a) and (2.2b). The result is

$$\mathcal{D} \times \boldsymbol{E} = i\omega\mu \boldsymbol{H}, \tag{2.4a}$$

$$\mathcal{D} \times \boldsymbol{H} = -i\omega\boldsymbol{\epsilon}\boldsymbol{E}, \qquad (2.4\text{b})$$

where $\mathcal{D}$ is the operator

$$\mathcal{D} \equiv \boldsymbol{\nabla} - ik\boldsymbol{\beta}(\boldsymbol{r}), \quad k = \omega/c, \quad \boldsymbol{\beta}(\boldsymbol{r}) = c^{-1}\boldsymbol{\Omega} \times \boldsymbol{r}. \quad (2.5)$$

We follow now the standard procedure of deriving the wave equation for $\boldsymbol{H}$, with $\mathcal{D}$ replacing $\boldsymbol{\nabla}$. The resulting equation is $\mathcal{D} \times (1/\epsilon_r)\mathcal{D} \times \boldsymbol{H} = k^2\boldsymbol{H}$. Collecting terms that are first order only (with respect to the angular velocity) and rearranging, we end up with our proposed wave equation in the rotating-medium rest frame, governing the magnetic field $\boldsymbol{H}_\Omega(r)$[1]:

$$\Theta\boldsymbol{H}_\Omega(\boldsymbol{r}) = k^2\boldsymbol{H}_\Omega(\boldsymbol{r}) + ik\mathbf{L}_\Omega\boldsymbol{H}_\Omega(\boldsymbol{r}). \qquad (2.6)$$

Here, Θ is the wave operator,

$$\Theta \equiv \boldsymbol{\nabla} \times \frac{1}{\epsilon_r(\boldsymbol{r})}\boldsymbol{\nabla} \times , \qquad (2.6\text{a})$$

and $\mathbf{L}_\Omega$ is the rotation-induced operator,

$$\mathbf{L}_\Omega\boldsymbol{H} = \boldsymbol{\nabla} \times \frac{\boldsymbol{\beta}(\boldsymbol{r})}{\epsilon_r(\boldsymbol{r})} \times \boldsymbol{H} + \frac{\boldsymbol{\beta}(\boldsymbol{r})}{\epsilon_r(\boldsymbol{r})} \times \boldsymbol{\nabla} \times \boldsymbol{H}, \qquad (2.6\text{b})$$

where $\boldsymbol{\beta}(\boldsymbol{r})$ is defined in Eqs. (2.5). In the development of Eqs. (2.6) and (2.6b), only terms up to the first order in $\boldsymbol{\beta}$ were kept.[1,7] Note that, when no rotation takes place, $\mathbf{L}_\Omega$ vanishes, and Eq. (2.6) reduces to the well-known stationary-medium wave equation.

Suppose now that we deal with a dielectric structure that contains a cavity. Suppose further that, at rest ($\Omega = 0$), this cavity resonates at frequency ω_0, at which M-order mode degeneracy is supported. Denote the degenerate modes by $\boldsymbol{H}_0^{(m)}(\boldsymbol{r})$, $m = 1, 2, \ldots M$. For these modes, Eq. (2.6) can be rewritten as

$$\Theta\boldsymbol{H}_0^{(m)}(\boldsymbol{r}) = k_0^2\boldsymbol{H}_0^{(m)}(\boldsymbol{r}), \quad k_0 = \omega_0/c, \quad m = 1, 2, \ldots, M. \qquad (2.7)$$

From the mathematical point of view, our goal now is to express the resonant frequency and resonant field under rotation $(\omega, \boldsymbol{H}_\Omega)$ governed by Eq. (2.6), in terms of the resonant frequency and modes of the system at rest $(\omega_0, \boldsymbol{H}_0^{(m)})$. Toward this end, we define the inner product between two vector fields as the volume integration

$$\langle\boldsymbol{F}, \boldsymbol{G}\rangle \equiv \int \boldsymbol{F} \cdot \bar{\boldsymbol{G}}\mathrm{d}^3\boldsymbol{r}, \qquad (2.8)$$

where the overline denotes the complex conjugate and $\boldsymbol{F} \cdot \boldsymbol{G}$ is the standard scalar product between the two vectors $\boldsymbol{F}$ and $\boldsymbol{G}$. Perform now an inner product of Eq. (2.7) with $\boldsymbol{H}_\Omega$, and of Eq. (2.6) with each of the degenerate modes $\boldsymbol{H}_0^{(m)}$. The result is the following set of equations:

$$\langle\Theta\boldsymbol{H}_0^{(m)}, \boldsymbol{H}_\Omega\rangle = k_0^2\langle\boldsymbol{H}_0^{(m)}, \boldsymbol{H}_\Omega\rangle,$$

$$\langle\Theta\boldsymbol{H}_\Omega, \boldsymbol{H}_0^{(m)}\rangle = k^2\langle\boldsymbol{H}_\Omega, \boldsymbol{H}_0^{(m)}\rangle$$

$$+ ik\langle\mathbf{L}_\Omega\boldsymbol{H}_\Omega, \boldsymbol{H}_0^{(m)}\rangle, \qquad (2.9)$$

which hold for $m = 1, \ldots, M$. By subtracting from the second equation above the complex conjugate of the first one

and using the fact that Θ is a self-adjoint operator, we obtain

$$(k^2 - k_0^2)\langle\boldsymbol{H}_\Omega, \boldsymbol{H}_0^{(m)}\rangle + ik\langle\mathbf{L}_\Omega\boldsymbol{H}_\Omega, \boldsymbol{H}_0^{(m)}\rangle = 0, \quad m = 1, 2, \ldots M. \qquad (2.10)$$

It is well known that slow rotation may affect the phase accumulation rates and the resonant frequency, but its effect on the modes' shape is completely negligible.[9] Thus, we express $\boldsymbol{H}_\Omega$ as a summation over the stationary modes:

$$\boldsymbol{H}_\Omega(\boldsymbol{r}) = \sum_{n=1}^{M} a_n\boldsymbol{H}_0^{(n)}(\boldsymbol{r}). \qquad (2.11)$$

Substituting this back into Eq. (2.10), we obtain the matrix equation

$$(k^2 - k_0^2)\sum_{n=1}^{M} a_n A_{mn} = -ik\sum_{n=1}^{M} a_n\langle\mathbf{L}_\Omega\boldsymbol{H}_0^{(n)}, \boldsymbol{H}_0^{(m)}\rangle,$$

$$m = 1, 2, \ldots M, \qquad (2.12)$$

where

$$A_{mn} = \langle\boldsymbol{H}_0^{(n)}, \boldsymbol{H}_0^{(m)}\rangle. \qquad (2.12\text{a})$$

The inner-product terms in the right-hand side of Eq. (2.12) above incorporate the effect of rotation via the operator $\mathbf{L}_\Omega$. Similar expressions were obtained and simplified in a previous work on the subject.[1] Using the same procedure, with the slight generalization that here the modal fields $\boldsymbol{H}_0^{(n)}$ are not assumed to be real (see Appendix A for details), we obtain the following simplified expression:

$$\langle\mathbf{L}_\Omega\boldsymbol{H}_0^{(n)}, \boldsymbol{H}_0^{(m)}\rangle = ic^{-1}\Omega\omega_0 B_{mn}, \qquad (2.13)$$

where

$$B_{mn} = \epsilon_0\langle\hat{z} \times \boldsymbol{r}, \bar{\boldsymbol{H}}_0^{(n)} \times \boldsymbol{E}_0^{(m)} + \boldsymbol{H}_0^{(m)} \times \bar{\boldsymbol{E}}_0^{(n)}\rangle. \quad (2.13\text{a})$$

Define now $\mathbf{A}$ and $\mathbf{B}$ as square $M \times M$ matrices with elements A_{mn} and B_{mn}, respectively. Since the degenerate modes $\boldsymbol{H}_0^{(m)}$ are linearly independent, $\mathbf{A}$ is nonsingular, so its inverse $\mathbf{A}^{-1}$ exists. Therefore Eq. (2.12) can be written as the eigenvalue problem

$$\Omega\mathbf{A}^{-1}\mathbf{B}\boldsymbol{a} = \frac{\omega^2 - \omega_0^2}{\omega\omega_0}\boldsymbol{a}, \quad \boldsymbol{a} = \begin{pmatrix} a_1 \\ a_2 \\ \vdots \\ a_M \end{pmatrix}, \qquad (2.14\text{a})$$

where $\boldsymbol{a}$ is a column vector with the elements a_n. It is clear that, at slow rotation, the splitting of ω_0 into different resonances ω is small. Thus we write

$$\omega = \omega_0 + \delta\omega, \qquad (2.15\text{a})$$

and, up to first order in $\delta\omega/\omega_0$, we can approximate ($\omega^2 - \omega_0^2 \approx 2\omega_0\delta\omega$):

$$\frac{\omega^2 - \omega_0^2}{\omega\omega_0} \approx 2\frac{\delta\omega}{\omega_0}. \qquad (2.15\text{b})$$

The eigenvalue problem in Eq. (2.14a) can be rewritten as

$$\mathbf{C}\boldsymbol{a} = \frac{\delta\omega}{\omega_0\Omega}\boldsymbol{a}, \quad \mathbf{C} = (1/2)\mathbf{A}^{-1}\mathbf{B}. \qquad (2.16)$$

Generally, the matrix $\mathbf{C}$ possesses M distinct eigenvalues Λ_j, $j=1,\ldots M$. As we shall see in Subsection 2.B.1, these eigenvalues are real. Therefore the last equation yields the following M values of frequency splitting:

$$\delta\omega_j(\Omega) = \Omega\omega_0\Lambda_j, \quad j=1,\ldots,M. \qquad (2.17)$$

Furthermore, each eigenvalue Λ_j corresponds to an eigenvector $\boldsymbol{a}^j$, whose elements $(\boldsymbol{a}^j)_n$, $n=1,\ldots M$, can be used in Eq. (2.11) to approximate the jth splitted mode of the rotating microcavity. Additional properties of the eigenvalue problem that will be useful in the analysis of Section 3 are described below.

A. Symmetries, Realness of the Eigenvalues, and Interpretation of $\mathbf{A}^{-1}\mathbf{B}$

It is easily verified that the matrices $\mathbf{A}$ and $\mathbf{B}$ are self-adjoint; namely, they possess the symmetry properties

$$A_{mn} = \bar{A}_{nm}, \quad B_{mn} = \bar{B}_{nm}, \qquad (2.18a)$$

and the diagonal elements of $\mathbf{B}$ are given by

$$B_{mm} = -2\epsilon_0\langle\hat{z}\times\boldsymbol{r}, \mathrm{Re}\,\boldsymbol{S}_0^{(m)}\rangle. \qquad (2.18b)$$

Here $\boldsymbol{S}_0^{(m)} = \boldsymbol{E}_0^{(m)}\times\bar{\boldsymbol{H}}_0^{(m)}$ is the Poynting vector of the cavity's mth mode.

Since the inverse of a self-adjoint operator is self-adjoint, it follows that $\mathbf{A}^{-1}$ is self-adjoint, too [see comment after Eq. (2.13a)]. A product of self-adjoint operators is a self-adjoint operator. Thus $\mathbf{A}^{-1}\mathbf{B}$ is self-adjoint and possesses pure real eigenvalues. This proves the realness of the Λ_j's in Eq. (2.17).

It is instructive to examine more closely the integrand u_{mn} associated with the elements B_{mn}. In cylindrical coordinates, we have $\hat{z}\times\boldsymbol{r} = |\boldsymbol{r}|\hat{\phi}$. Then

$$B_{mn} = \epsilon_0\int_V u_{mn}\mathrm{d}^3r$$

$$= \epsilon_0\int_V |\boldsymbol{r}|\hat{\phi}\cdot(\boldsymbol{H}_0^{(n)}\times\bar{\boldsymbol{E}}_0^{(m)} + \bar{\boldsymbol{H}}_0^{(m)}\times\boldsymbol{E}_0^{(n)})\mathrm{d}^3r. \qquad (2.18c)$$

Thus, up to a multiplicative factor, the operator $\mathbf{A}^{-1}\mathbf{B}$ can be interpreted as an operator that extracts the effective radius of the power rotation (along $\hat{\phi}$), carried mutually by the modes inside the cavity. This will be demonstrated in the following subsections.

Finally, we note that a great deal of simplification in the interpretation of the results and further physical insights are gained if one uses an orthogonal and real set $\boldsymbol{H}_0^{(m)}$. This is discussed in the following.

B. Using Orthogonal and Real Set $\boldsymbol{H}_0^{(m)}$

The degenerate modes $\boldsymbol{H}_0^{(m)}$ satisfying Eq. (2.7) are linearly independent. Furthermore, since they all possess

the same eigenvalue k_0^2, any linear combination of degenerate modes is by itself a degenerate mode. It follows from the above arguments that, without loss of generality, we can always assume that the functions $\boldsymbol{H}_0^{(m)}$, $m=1,\ldots,M$, constitute an orthogonal set (i.e., we can apply the Gram–Schmidt procedure, if necessary). Therefore, we get

$$\mathbf{A} = \|\boldsymbol{H}_0^{(1)}\|^2\mathbf{I}, \qquad (2.19)$$

where $\mathbf{I}$ is the identity matrix. Note that, in principle, owing to normalization we can have $\mathbf{A}=\mathbf{I}$, but the generic term $\|\boldsymbol{H}_0^{(1)}\|$ is kept in order to avoid confusion with physical units. In addition, since the operator in Eq. (2.7) is self-adjoint, the eigenvalue k_0^2 is real, and the corresponding degenerate modes $\boldsymbol{H}_0^{(m)}$ can always be normalized such that they constitute pure real functions (if a generally complex $\boldsymbol{H}_0^{(m)}$ constitutes a mode, so does $\mathrm{Re}\,\boldsymbol{H}_0^{(m)}$.) Then $\boldsymbol{E}_0^{(m)}$ must be pure imaginary [$\nabla\times\boldsymbol{H}_0^{(m)} = -i\omega_0\epsilon_0\epsilon_r(\boldsymbol{r})\boldsymbol{E}_0^{(m)}$], making $\mathbf{B}$ pure imaginary with a vanishing diagonal [see Eqs. (2.13a) and (2.18b)]. Therefore $\mathbf{C}$ is of the form

$$\mathbf{C} = \frac{1}{2\|\boldsymbol{H}_0^{(1)}\|^2}\begin{bmatrix} 0 & B_{12} & B_{13} & \cdots & B_{1M} \\ \bar{B}_{12} & 0 & B_{23} & \cdots & B_{2M} \\ \bar{B}_{13} & \bar{B}_{23} & 0 & \cdots & B_{3M} \\ \vdots & & & & \\ \bar{B}_{1M} & \bar{B}_{2M}\cdots & & & 0 \end{bmatrix} \equiv i\boldsymbol{\Gamma},$$

$$(2.20)$$

where $\boldsymbol{\Gamma}$ is a real skew-symmetric matrix[10] (a real matrix whose elements satisfy $\gamma_{mn} = -\gamma_{nm}$ and $\gamma_{nn}=0$). Real $M\times M$ skew-symmetric matrices satisfy the following interesting properties, listed together with their important implications for our problem:

(i) If M is even, the eigenvalues are pure imaginary and always come in symmetric pairs around the origin: $\pm i\Lambda$. Hence Λ, the eigenvalues of $\mathbf{C}$, are real and symmetric around the origin. This means that the degenerate modes always undergo a symmetrical split of their resonance frequency.

(ii) If M is odd, the rule above still applies, except that there is an additional eigenvalue at the origin: $\Lambda=0$. Hence, a degenerate mode whose resonant frequency does not change under rotation exists if the system possesses odd-order degeneracy.

The above results may offer the following physical interpretation. The rotating system possesses M modal solutions $\boldsymbol{H}_\Omega(\boldsymbol{r})$ that are obtained eventually by the summation in Eq. (2.11), where the summation coefficients are nothing but the elements of the eigenvectors $\boldsymbol{a}$ of the rotation operator [see Eqs. (2.16)]. Generally, this summation yields new modes $\boldsymbol{H}_\Omega$ that rotate around the cavity center and correspond effectively to azimuthal propagation within the cavity. The new modes that corotate (counterrotate) with Ω undergo a downward (upward) shift in their resonant frequency and correspond to the negative (positive) eigenvalues Λ. Furthermore, owing to the symmetry of the matrices involved, to every clockwise-

rotating new mode $\boldsymbol{H}_\Omega$ there corresponds a counterclockwise-rotating new mode with an identical field structure. Hence the symmetrical frequency splitting results. However, if M is odd, there exists one additional mode corresponding to radial propagation (i.e., from the cavity center outward toward the cavity walls and back to the center). Such propagation is not affected by rotation (up to first order in $\boldsymbol{\Omega}$), hence the zero eigenvalue of the rotation operator. Clearly, a conventional cavity (no mode degeneracy) is a special case that corresponds to $M=1$ and up to first order in Ω is not affected by rotation.

Another example of an odd-order degeneracy can be provided by a cavity in a three-dimensional crystal. If $\boldsymbol{\Omega} = \hat{z}\Omega$, then a zero-eigenvalue mode corresponds to a field oscillating along the z axis and possessing azimuthal symmetry in the (x,y) plane.

Comment. How general are the results discussed above? It should be emphasized that the only assumption made is the use of the orthogonal and real set for $\boldsymbol{H}_0^{(m)}$. However, since generally degenerate modes are linearly independent, the passage from any arbitrary set of m degenerate modes of the system to a real and orthogonal set is nothing but a change of basis. Such transformation does not affect the spectral properties of the matrices involved. Therefore the conclusions discussed above, especially those pertaining to the location of eigenvalues and their interpretations, are of general validity and are not restricted to a specific set of degenerate modes.

C. Case of $M=2$
The properties of the eigenvalues Λ_j and the corresponding eigenvectors $\boldsymbol{a}^j$ are seen most transparently for the case of the second-order degeneracy. This case is often encountered in PhC (see, for example, Figs. 1(c), 1(d), and 6). Here the degenerate orthogonal modes $\boldsymbol{H}_0^{1,2}(\boldsymbol{r})$ can be viewed as two dipoles with an angle of $\pi/2$ between their polarizations.

With respect to the eigenvalues of Eq. (2.20) above for $M=2$, it can be shown by a straightforward algebraic calculation that

$$\Lambda_{1,2} = \pm \frac{|B_{12}|}{2\|\boldsymbol{H}_0^{(1)}\|^2}, \tag{2.21}$$

and the corresponding eigenvectors $\boldsymbol{a}^{(1,2)}$ satisfy

$$(\boldsymbol{a}^{(1,2)})_1 = \mp i(\boldsymbol{a}^{(1,2)})_2, \tag{2.22}$$

where $(\boldsymbol{a}^j)_n$ is the nth element of the jth. eigenvector. This result is physically illuminating. It shows that the modal fields $\boldsymbol{H}_\Omega$ of the rotating system are obtained by a superposition of $\boldsymbol{H}_0^{(1)}(\boldsymbol{r})$ and $\boldsymbol{H}_0^{(2)}(\boldsymbol{r})$ with a phase difference of $\pm\pi/2$. This superposition yields a rotating mode; the two modes of the rotating system rotate clockwise and counterclockwise, and each possesses a shift of its resonance (i.e., splitting) according to a generalized Sagnac effect. This result is consistent with the physical interpretation as discussed in Subsection 2.B.

3. CLASSICAL SAGNAC EFFECT AND EFFECTIVE ROTATION RADIUS
The theory developed in the previous sections holds for a general cavity that supports degenerate modes. It therefore should hold also for the simplest and most familiar example: the ring resonator. For large rings (rings of radius R large compared with the wavelength), the classical Sagnac effect formula predicts the frequency splitting $\omega^{(1,2)} = \omega_0 \pm \omega_0 R/(nc)$. We show that our theory reconstructs this classical expression.

For a large ring, the electric and magnetic fields of the degenerate modes are most easily presented as clockwise and counterclockwise propagating local plane waves of the following form:

$$\boldsymbol{E}_0^{(1,2)} = \hat{z}\,\eta H_0 \exp(\pm ik_0 nR\phi), \tag{3.1a}$$

$$\boldsymbol{H}_0^{(1,2)} = \pm\hat{\rho}H_0 \exp(\pm ik_0 nR\phi), \tag{3.1b}$$

where $n = \sqrt{\epsilon_r}$ and $\eta = \sqrt{\mu_0/\epsilon_0\epsilon_r}$. At this point it should be noted that one can transform these fields into their real-orthonormal counterparts as discussed in Subsection 2.B. The result is two standing waves expressed as cosine and sine functions. However, as emphasized before, the final results are independent of the specific form of the modal set. Thus, for the present simple example we prefer to keep the complex form. For a ring of width small compared with its radius R, we can now approximate B_{11} by

$$B_{11} \approx \epsilon_0 R\langle\hat{\phi}, -\hat{\phi}\bar{H}_0 E_0 - \hat{\phi}H_0\bar{E}_0\rangle = -2\epsilon_0 R\|\boldsymbol{H}_0\|^2\eta. \tag{3.2}$$

Likewise, $B_{22} = 2\epsilon_0 R\|\boldsymbol{H}_0\|^2\eta$, $B_{12} = B_{21} = 0$, and $\mathbf{A} = I\|\boldsymbol{H}_0\|^2$. This yields

$$\mathbf{C} = \frac{R}{nc}\begin{bmatrix} -1 & 0 \\ 0 & 1 \end{bmatrix}, \tag{3.3}$$

for which $\Lambda_{1,2} = \pm R/(nc)$. Thus

$$\delta\omega_{12} = \omega_0\Omega\Lambda_{12} = \pm\omega_0\Omega R/(nc), \tag{3.4}$$

that is, as predicted, the classical Sagnac effect.[4]

Comment: The effective radius. The last result offers the concept of an effective radius of rotation for the most general case of degenerate modes. The effective rotation radius of the ith mode, possessing the eigenvalue Λ_i, is given by

$$R_i^{\mathrm{eff}} = |\Lambda_i|nc. \tag{3.5}$$

As we show in Section 4, this expression indeed yields the radius of annular domain in the cavity that contributes the most to the frequency splitting and is consistent with the interpretation discussed in connection with Eq. (2.18c).

4. EXAMPLE OF A ROTATING PHOTONIC CRYSTAL

The first structure under consideration is shown in Fig. 2. It is a two-dimensional crystal consisting of 91 dielectric cylinders of radius 0.6 μm and $\epsilon_r = 8.41$, with a hexagonal lattice with a lattice constant of $a = 4$ μm. For the TM po-
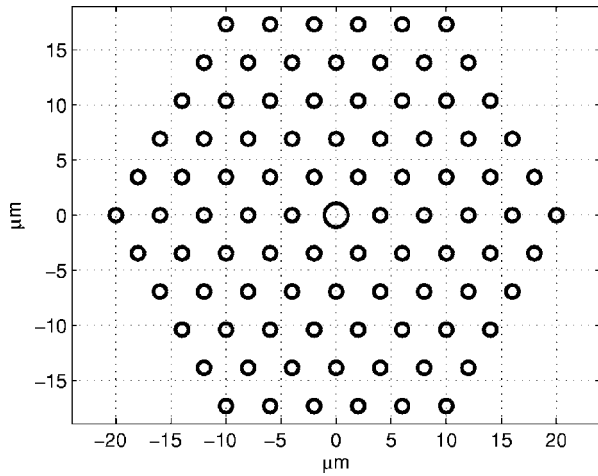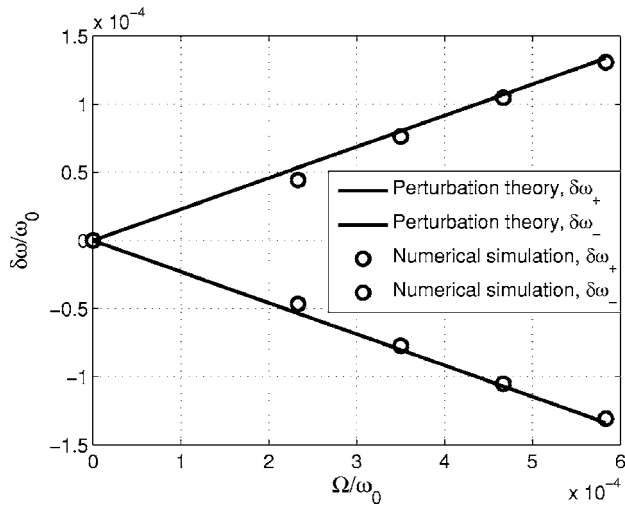
Fig. 2.   PhC structure under study.

Fig. 3.   Splitting of the degenerate cavity resonance frequency due to rotation.

larization, this structure possesses a bandgap covering the range between 7.5 and 10.5 μm. A microcavity with degeneracy rank $M=2$ (i.e., supporting two degenerate modes) at a resonant wavelength of $\lambda_0 = 2\pi c/\omega_0$ = 8.79941 μm is created at the center by increasing the radius of the central cylinder to 1.1 μm. The degenerate modes' electric field magnitude is shown in Fig. 1.

Below we demonstrate the effect of rotation on the structure. We first calculate the mode splitting due to rotation by using the theory developed here and then compare the results with those obtained by full numerical simulation of the rotating crystal.

A. Theoretical Prediction

The degenerate modal fields of the stationary structure, $E_0^{(1,2)}$, $H_0^{(1,2)}$ shown in Fig. 1, were obtained numerically by our exciting the structure under study (Fig. 2) with incident plane waves of wavelength $\lambda_0 = 2\pi c/\omega_0 = 8.79941$ μm and solving for the fields using a method-of-moments[11]-based approach—the multifilament algorithm.[12,13] Owing to the strong isolation of the microcavity, obtained by the surrounding crystal, the fields within the cavity and in its close neighborhood constitute a good approximation of the true modal fields of the structure. These numerically obtained stationary-system fields were substituted into the theoretical expressions in Eqs. (2.12a) and (2.13a) in order to compute the matrices $\mathbf{A}$ and $\mathbf{B}$, and then the eigenvalues $\Lambda_{1,2}$ were calculated. The result is $\omega_0 \Lambda_{1,2} = \pm 0.229$, and Fig. 3 shows the corresponding resonance splitting, obtained by our substituting this result into Eq. (2.17) (solid lines).

According to Eq. (3.5), the effective rotation radius of the microcavity in the present example is 0.93 μm. It is instructive to check this number against a plot of the integrand of B_{12} and B_{21} in the x,y plane [see discussion after Eq. (2.18c)]. The integrands u_{12} and u_{21} are shown in
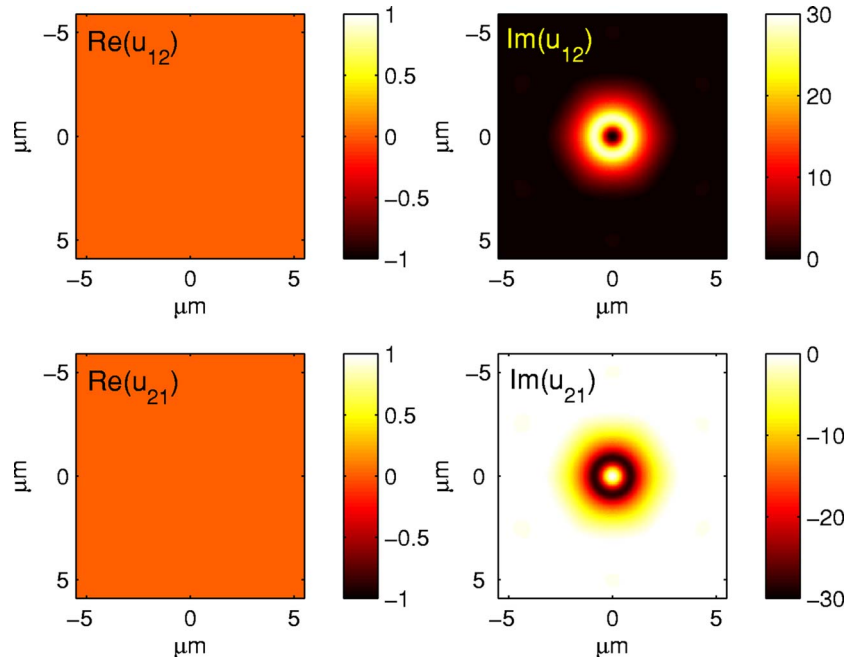

Fig. 4.   (Color online) The integrand in Eq. (2.18c) used to compute the elements of $\mathbf{B}$. The mode functions shown in Figs. 1(c) and 1(d) are used.

Fig. 4. As predicted, these functions are pure imaginary and are essentially concentrated along a circular path whose radius is about 1 μm. This value is consistent with the effective radius calculation using Eq. (3.5).

B. Full Numerical Simulation of the Rotating System

1. Algorithm Considerations

Our system consists of a high-Q resonator. Thus, direct time-domain approaches such as the finite-difference time domain may suffer from slow convergence and enhanced numerical dispersion effects. We note that, at the rest frame of the rotating system, the optical signal possesses a pure time-harmonic nature. Thus, a good candidate for a numerical computation of the entire scenario is a moment-method-based time-harmonic algorithm.[11] A vital ingredient of any such algorithm is the Green's function $G(\boldsymbol{r}, \boldsymbol{r}')$ of an appropriately defined background medium, describing the field at $\boldsymbol{r}$ due to a unit point source at $\boldsymbol{r}'$. For scattering from a stationary structure, the background is most conveniently defined as a homogeneous medium, and the corresponding G is well known. For analysis of scattering from a rotating structure, as seen in the rotating-medium rest frame, the background-problem Green's function $G^{\Omega}(\boldsymbol{r}, \boldsymbol{r}')$ is the field in a rotating homogeneous medium in which both the source point at $\boldsymbol{r}'$ and the observer at $\boldsymbol{r}$ rotate together with the medium at an angular velocity $\hat{z}\Omega$. For two-dimensional problems, $G\Omega(\boldsymbol{r}, \boldsymbol{r}')$ has been studied in detail in a recent work.[3] It can be expressed in cylindrical coordinates as

$$G^{\Omega} = I \frac{i}{4} \sum_{m=-\infty}^{\infty} J_m(k_0 n \gamma_m \rho_<) H_m^{(1)}(k_0 n \gamma_m \rho_>) \exp[im(\theta - \theta^1)]$$

$$\approx I \frac{i}{4} H_0^{(1)} \exp\left[i \frac{\Omega}{\omega} k_0^2 (yx' - xy')\right], \qquad (4.1)$$

where $I = i\omega\mu$ or $I = i\omega\epsilon$ for TM or TE polarization, $H_m^{(1)}$ is the mth-order Hankel function of the first kind, J_m is the mth-order Bessel function, $\gamma_m = [1 + 2m\Omega/(\omega n^2)]^{1/2}$, and $\rho_>, \rho_< = \max, \min(\rho, \rho')$. With this at hand, well-tested legacy codes dealing traditionally with stationary scatterers can be extended to hold also for rotating scatterers (at their rest frame), simply by one's replacing the stationary-medium Green's function by G^{Ω} and at no additional cost of algorithm complexity or programming. [It is easily verified that in two-dimensional geometries rotation does not affect boundary conditions at the dielectric interface[3]; this can be seen directly from the divergence-free conditions in Eqs. (2.2a) and (2.2b) by one's applying to it the fact that the structure is invariant along the rotation axis $\hat{z}$.] With this approach, we have extended the multifilament method (used, for example, in Ref. 2 and references therein) to apply to rotating crystals as well.

2. Numerical Results

We used the rotating-medium algorithm to simulate the entire structure of Fig. 2 under rotation. The system was excited by an incident plane wave, and the field intensity inside the cavity as a function of the excitation wavelength has been computed for various values of Ω. The rotation frequency has been extremely exaggerated in order to resolve the resonance splitting at a reasonable numeri-

cal effort; we choose Ω/ω_0 of the order of 10^{-5}. The results are shown in Fig. 5. At rest ($\Omega/\omega_0 = 0$), the intensity graph peaks exactly at the resonance wavelength $\lambda_0 = 8.79941 \mu$m. Note that the resonance relative bandwidth ($\Delta\lambda/\lambda_0$) is about 10^{-4}. This relatively low-Q resonance ($Q \approx 10^4$) is mainly due to the finite size of the crystal and to numerical inaccuracy. Thus, in simulating the rotating crystal, one has to choose rotation speeds sufficiently large to yield resonance splitting larger than $Q^{-1} = \Delta\lambda/\lambda_0$ (in relative terms) in order to resolve the effect numerically (see discussion regarding the practical implications of this issue in Section 6). This is the main reason for choosing high rotation speeds. As can be seen from the graph, as Ω increases, two peaks can be identified, each of which corresponds to a distinct resonance. The distance of each of these peaks from the resonance of the stationary system—the splitting due to rotation—has been extracted and is displayed in Fig. 3 as a function of the normalized rotation rate Ω/ω_0 (circles). The figure also displays the splitting as predicted by the analytical results (solid line). As can be seen, there is a good agreement between the results.

5. MODEL FOR ROTATING SLAB PHOTONIC CRYSTAL MICROCAVITY

The second structure under consideration is the slab photonic crystal (PhC) microcavity discussed in several previous works[5,6] and operating at the 1.55 μm range. An optically thin slab made of InGaAsP ($\epsilon_r = 3.4$ at vacuum wavelength $\lambda_v = 1.55 \mu$m), with a thickness of half material wavelength, supports a fundamental TE mode whose effective index is approximately 2.64. To create a realistic PhC, the slab is patterned by a two-dimensional hexagonal array of air holes, and a microcavity is created by filling up one of the air holes with the slab material (removing a hole). It has been shown[5] that, for the range of frequencies that correspond to the fundamental TE mode of the slab, this structure can be modeled quite accurately by using a much simpler ideal two-dimensional model. The simplified model consists of an ideal two-dimensional crystal with the same air-hole geometry as that of the
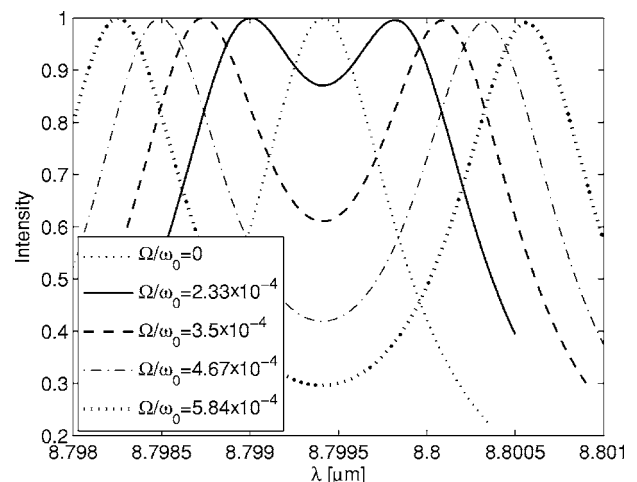

Fig. 5. Intensity of the field inside the rotating cavity versus excitation wavelength, for various values of the angular velocity Ω.

slab, embedded in a background medium possessing the effective property; $\epsilon_r = 2.64$. Thus, we consider a hexagonal lattice of air holes of radius 0.14 μm and a lattice constant of 0.475 μm, in a material with $\epsilon_r = 2.64$. A microcavity is created by filling in one of the air holes by the background material. For TE polarization, this cavity resonates at $\lambda_0 = 1.5548$ μm, supporting two degenerate modes (see Ref. 5 for details and for the modes' shapes).

We have repeated the computations detailed in Section 4 for the present structure. The results are summarized in Fig. 6. The stationary-system modal fields $E_0^{(1,2)}$, $H_0^{(1,2)}$ were computed numerically, and then the eigenvalues $\Lambda_{1,2}$ were calculated using the formulation in Section 2. The result is $\omega_0 \Lambda_{1,2} = \pm 0.0522$, and Fig. 6 shows the corresponding resonance splitting, obtained by substituting this result into Eq. (2.17) (solid lines). Next, full numerical simulations of the rotating system, as discussed in Subsection 4.B, were performed with extremely exaggerated rotation speeds for easy numerical extraction of the resonance splitting (Q here is about 50 times smaller than that of the example in Subsection 4.B—see discussion in Subsection 4.B.2). A computation similar to the one shown in Fig. 5 but for the TE slab model was performed, and the extracted maxima are shown in Fig. 6 by circles.

6. IMPLEMENTATION CONSIDERATIONS

The aim of the present work is to carry out a detailed theoretical study of the rotation-induced splitting of mode degeneracy in microcavities with sizes of the order of one wavelength. It is clear that its implementation to practical optical gyroscopes constitutes a research subject by itself. Nevertheless, the present study can provide some observations.

First, it is important to recognize that, in general, the lack of uniformity or stability of any gyroscope's environmental conditions is an important factor that eventually limits its resolution. Therefore, it is clear that miniaturization is potentially advantageous; hence the motivation to minimize the gyroscope dimensions. In this respect, note that the geometry of the second example (discussed
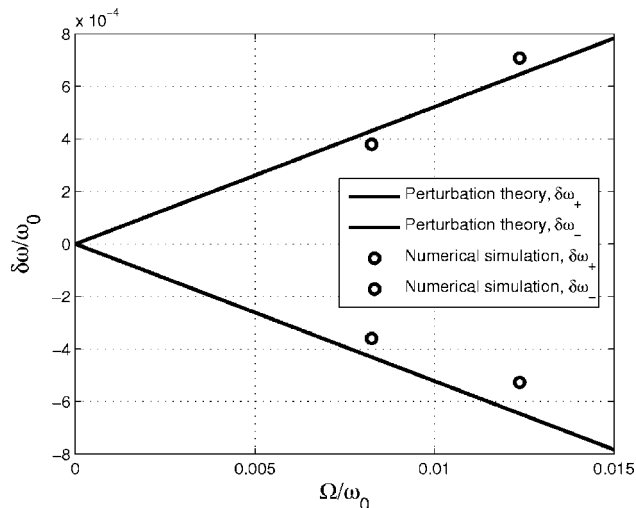

Fig. 6.   Splitting of the degenerate cavity resonance frequency due to rotation, for the slab PhC (TE polarization).

in Section 5) is almost an order of magnitude smaller in diameter than that of the first example (Section 4). However, its sensitivity to rotation, as implied by the magnitude of the eigenvalues $\Lambda_{1,2}$, is smaller only by a factor of 4 ($\omega_0|\Lambda| = 0.229$ and 0.0522 in the first and second examples, respectively). This observation suggests that, in principle, structure optimization can be invoked to obtain best performance in terms of sensitivity or dimensions.

The second point pertains to the detectability of the frequency splitting. It is clear that a frequency splitting that is smaller than the stationary-system bandwidth (where the latter scales as Q^{-1}) may be extremely difficult to detect and to measure. In such cases, the corresponding cavity excitation curve cannot be separated into two distinct resonance peaks. Let $\Delta\omega$ be the cavity resonance bandwidth. Then a rough estimate of the smallest detectable rotation rate Ω_{min} is given by [see Eq. (2.17)]

$$\Omega_{min} = \frac{\Delta\omega}{\omega_0 \max_j \Lambda_j} \approx \frac{1}{Q \max_j \Lambda_j}, \qquad (6.1)$$

where in the second equality we used $\Delta\omega/\omega_0 \approx Q^{-1}$, which holds for passive resonators. Thus, for practical designs, one should employ extremely high-Q microcavities; values of $Q \approx 10^4$ may suffice for a principle theoretical demonstration (as done in this work), but they certainly fall short of what is needed for a practical implementation. However, intensive research efforts carried on currently by many groups are aimed toward increasing the Q of microcavities.[5,6,14,15] Recently,[15] PhC microcavities with quality factors of the order of 10^6 were fabricated, and theoretical estimations indicating that values of Q exceeding 2×10^7 are possible were reported. In a different configuration, microcavities of the toroid structure with $Q = 10^8$ were fabricated.[16] These resonators support mode degeneracy and resonant splitting under rotation just as well and are amenable to the same study carried out here. Furthermore, all these achievements have been accomplished for passive microcavities. It is well known that the presence of gain material and lasing may further increase the quality factor (or decrease bandwidth) by several orders of magnitude. Thus, while certainly not an easy task, it is anticipated that the Q factors (or bandwidth) required for practical gyroscope implementations will eventually be achieved.

Finally, we note that the work in Ref. 1 studied theoretically the effect of rotation on a closed-loop CCW, known also as a coupled-resonator optical waveguide (CROW). It has been shown theoretically that a compact optical gyroscope can be designed on the basis of that scheme. This work[1] assumes that the microcavities constituting the waveguide do not support mode degeneracy. New studies, however, show that the presence of mode degeneracy can be exploited to enhance the device sensitivity[17–19]; it has been shown that CROWs consisting of microcavities with mode degeneracy can exhibit exponential-type sensitivity to rotation.[18,19] A pivotal ingredient in these new devices is the rotation-induced splitting reported here. This subject is currently under further investigations.

7. CONCLUSION

A theory for slowly rotating microcavities that support mode degeneracy has been developed. It was shown that rotation induces splitting of the (stationary system) degenerate resonance frequency ω_0 to several frequencies, and a detailed theoretical study of this splitting effect has been carried out. The proposed theory recovers the classical Sagnac effect for the specific case of the large ring resonator. Furthermore, it provides a systematic framework for cases in which where the classical expressions of the Sagnac effect cannot be directly applied. In the most general case, Mth-order degeneracy undergoes splitting into M different resonances, symmetrically distributed around ω_0. The magnitude of the frequency splitting is linearly dependent on the rotation speed Ω, with proportionality factors given by the eigenvalues of the proposed rotation operator. The theory has been tested on specific examples of rotating photonic crystals' microcavities, and the splitting effect has been demonstrated. Implications to practical optical gyroscopes were discussed.

APPENDIX A: THE B_{mn} COEFFICIENTS

We have the following identities [use $(\nabla \times \boldsymbol{A}) \cdot \boldsymbol{B} = \nabla \cdot (\boldsymbol{A} \times \boldsymbol{B}) + \boldsymbol{A} \cdot (\nabla \times \boldsymbol{B})$ and $\boldsymbol{A} \cdot (\boldsymbol{B} \times \boldsymbol{C}) = (\boldsymbol{A} \times \boldsymbol{B}) \cdot \boldsymbol{C}$]:

$$\left(\nabla \times \frac{\boldsymbol{\beta}}{\epsilon_r} \times \boldsymbol{H}_0^{(n)} \right) \cdot \bar{\boldsymbol{H}}_0^{(m)} = \nabla \cdot \left[\left(\frac{\boldsymbol{\beta}}{\epsilon_r} \times \boldsymbol{H}_0^{(n)} \right) \times \bar{\boldsymbol{H}}_0^{(m)} \right]$$
$$+ \left(\frac{\boldsymbol{\beta}}{\epsilon_r} \times \boldsymbol{H}_0^{(n)} \right) \cdot (\nabla \times \bar{\boldsymbol{H}}_0^{(m)}),$$
(A1a)

$$\left(\frac{\boldsymbol{\beta}}{\epsilon_r} \times \nabla \times \boldsymbol{H}_0^{(n)} \right) \cdot \boldsymbol{H}_0^{(m)} = - \left(\frac{\boldsymbol{\beta}}{\epsilon_r} \times \bar{\boldsymbol{H}}_0^{(m)} \right) \cdot (\nabla \times \boldsymbol{H}_0^{(n)}).$$
(A1b)

The inner products in Eq. (2.12) are nothing but volume integrations (over arbitrarily large volume V) of the terms above. Using the Gauss theorem, we get for the contribution of the first term on the right-hand side of Eq. (A1a)

$$\int_V \nabla \cdot \left[\left(\frac{\boldsymbol{\beta}}{\epsilon_r} \times \boldsymbol{H}_0^{(n)} \right) \times \bar{\boldsymbol{H}}_0^{(m)} \right] \mathrm{d}^3 x$$
$$= \oint_{S = \partial V} \left[\left(\frac{\boldsymbol{\beta}}{\epsilon_r} \times \boldsymbol{H}_0^{(n)} \right) \times \bar{\boldsymbol{H}}_0^{(m)} \right] \cdot \mathrm{d}s \to 0. \quad (A2)$$

This is because the flux through the surface $S = \partial V$ vanishes as V becomes large (the functions $\boldsymbol{H}_0^{(n)}$ are exponentially decreasing). Therefore, the inner product terms eventually comprise

$$\langle \mathbf{L}_\Omega \boldsymbol{H}_0^{(n)}, \boldsymbol{H}_0^{(m)} \rangle = \left\langle \frac{\boldsymbol{\beta}}{\epsilon_r} \times \boldsymbol{H}_0^{(n)}, \nabla \times \boldsymbol{H}_0^{(m)} \right\rangle$$
$$- \left\langle \nabla \times \boldsymbol{H}_0^{(n)}, \frac{\boldsymbol{\beta}}{\epsilon_r} \times \boldsymbol{H}_0^{(m)} \right\rangle. \quad (A3)$$

Using again $(\boldsymbol{A} \times \boldsymbol{B}) \cdot \boldsymbol{C} = \boldsymbol{A} \cdot (\boldsymbol{B} \times \boldsymbol{C})$,

$$\langle \mathbf{L}_\Omega \boldsymbol{H}_0^{(n)}, \boldsymbol{H}_0^{(m)} \rangle = \left\langle \frac{\boldsymbol{\beta}}{\epsilon_r}, \bar{\boldsymbol{H}}_0^{(n)} \times \nabla \times \boldsymbol{H}_0^{(m)} \right\rangle$$
$$- \left\langle \frac{\boldsymbol{\beta}}{\epsilon_r}, \boldsymbol{H}_0^{(m)} \times \nabla \times \bar{\boldsymbol{H}}_0^{(n)} \right\rangle. \quad (A4)$$

Since $\boldsymbol{\beta} = \boldsymbol{\beta}(\boldsymbol{r}) = \boldsymbol{\Omega} \times \boldsymbol{r}/c$ and $\boldsymbol{\Omega} = \Omega \hat{z}$, the above result yields

$$\langle \mathbf{L}_\Omega \boldsymbol{H}_0^{(n)}, \boldsymbol{H}_0(m) \rangle$$
$$= c^{-1} \Omega \left\langle \frac{\hat{z} \times \boldsymbol{r}}{\epsilon_r}, \bar{\boldsymbol{H}}_0^{(n)} \times \nabla \times \boldsymbol{H}_0^{(m)} - \boldsymbol{H}_0^{(m)} \times \nabla \times \bar{\boldsymbol{H}}_0^{(n)} \right\rangle.$$
(A5)

Finally, we use $\nabla \times \boldsymbol{H}_0^{(m)} = -i \omega_0 \epsilon_0 \epsilon_r(\boldsymbol{r}) \boldsymbol{E}_0^{(m)}$ to obtain

$$\langle \mathbf{L}_\Omega \boldsymbol{H}_0^{(n)}, \boldsymbol{H}_0^{(m)} \rangle = i c^{-1} \Omega \omega_0 \epsilon_0 \langle \hat{z} \times \boldsymbol{r}, \bar{\boldsymbol{H}}_0^{(n)} \times \boldsymbol{E}_0^{(m)} + \boldsymbol{H}_0^{(m)} \times \bar{\boldsymbol{E}}_0^{(n)} \rangle.$$
(A6)

B. Z. Steinberg, the corresponding author, can be reached by e-mail at steinber@eng.tau.ac.il.

REFERENCES

1. B. Z. Steinberg, "Rotating photonic crystals: a medium for compact optical gyroscopes," Phys. Rev. E **71**, 056621 (2005).
2. B. Z. Steinberg, A. Boag, and R. Lisitsin, "Sensitivity analysis of narrowband photonic crystal filters and waveguides to structure variations and inaccuracy," J. Opt. Soc. Am. A **20**, 138–146 (2003).
3. B. Z. Steinberg, A. Shamir, and A. Boag, "Two-dimensional Green's function theory for the electrodynamics of a rotating medium," Phys. Rev. E **74**, 016608 (2006).
4. E. J. Post, "Sagnac effect," Rev. Mod. Phys. **39**, 475–493 (1967).
5. O. Painter, J. Vuckovic, and A. Scherer, "Defect modes of a two-dimensional photonic crystal in an optically thin dielectric slab," J. Opt. Soc. Am. B **16**, 275–285 (1999).
6. M. Loncar, M. Hochberg, A. Scherer, and Y. Qiu, "High quality factors and room-temperature lasing in a modified single-defect photonic crystal cavity," Opt. Lett. **29**, 721–723 (2004).
7. T. Shiozawa, "Phenomenological and electron-theoretical study of the electrodynamics of rotating systems," Proc. IEEE **61**, 1694–1702 (1973).
8. J. L. Anderson and J. W. Ryon, "Electromagnetic radiation in accelerated systems," Phys. Rev. **181**, 1765–1775 (1969).
9. H. J. Arditty and H. C. Lefevre, "Sagnac effect in fiber gyroscopes," Opt. Lett. **6**, 401–403 (1981).
10. P. Lancaster and M. Tismenetsky, *The Theory of Matrices*, 2nd ed. (Academic, 1985).
11. R. F. Harrington, *Field Computation by Moment Methods* (Krieger, 1982).
12. Y. Leviatan and A. Boag, "Analysis of electromagnetic scattering from dielectric cylinders using a multifilament current model," IEEE Trans. Antennas Propag. **35**, 1119–1127 (1987).
13. A. Boag, Y. Leviatan, and A. Boag, "Analysis of two-dimensional electromagnetic scattering from a periodic grating of cylinders using a hybrid current model," Radio Sci. **23**, 612–624 (1988).
14. B. S. Song, S. Noda, and T. Asano, "Photonic devices based on in-plane hetero photonic crystals," Science **300**, 1537–1542 (2003).
15. B. S. Song, S. Noda, T. Asano, and Y. Akahane, "Ultra-high-Q photonic double-heterostructure nanocavity," Nat. Mater. **4**, 207–210 (2005).
16. D. K. Armani, T. J. Kippenberg, S. M. Spillane, and K. J.

Vahala, "Ultra-high-Q toroid microcavity on a chip," Nature **421**, 925–928 (2003).

17. J. Scheuer and A. Yariv, "Sagnac effect in coupled-resonator slow-light waveguide structures," Phys. Rev. Lett. **96**, 053901 (2006).

18. B. Z. Steinberg, J. Scheuer, and A. Boag, "Slow-light waveguides with mode degeneracy: rotation-induced super structures and optical gyroscopes," in *Proceedings of Slow and Fast Light OSA Topical Meeting* (Optical Society of America, 2006), paper MB3.

19. B. Z. Steinberg, J. Scheuer, and A. Boag, "Rotation-induced super structure in slow-light waveguides with mode degeneracy," submitted to J. Opt. Soc. Am. B.